

# Demographics of Transition Discs in Ophiuchus and Taurus

Joan R. Najita<sup>1,2\*</sup>, Sean M. Andrews<sup>2</sup>, and James Muzerolle<sup>3</sup>

<sup>1</sup>*National Optical Astronomy Observatory, 950 Cherry Avenue, Tucson, AZ. 85719, USA*

<sup>2</sup>*Harvard-Smithsonian Center for Astrophysics, 60 Garden Street, Cambridge, MA 02138, USA*

<sup>3</sup>*Space Telescope Science Institute, 3700 San Martin Drive, Baltimore, Maryland 21218, USA*

## ABSTRACT

Transition disc systems are young stars that appear to be on the verge of dispersing their protoplanetary discs. We explore the nature of these systems by comparing the stellar accretion rates  $\dot{M}_*$  and disc masses  $M_d$  of transition discs and normal T Tauri stars in Taurus and Ophiuchus. After controlling for the known dependencies of  $\dot{M}_*$  and  $M_d$  on age,  $\dot{M}_*$  on stellar mass, and  $M_d$  on the presence of stellar or sub-stellar companions, we find that the normal T Tauri stars show a trend of  $\dot{M}_*$  increasing with  $M_d$ . The transition discs tend to have higher average disc masses than normal T Tauri stars as well as lower accretion rates than normal T Tauri stars of the same disc mass. These results are most consistent with the interpretation that the transition discs have formed objects massive enough to alter the accretion flow, i.e., single or multiple giant planets. Several Ophiuchus T Tauri stars that are not known transition disc systems also have very low accretion rates for their disc masses. We speculate on the possible nature of these sources.

**Key words:** planets and satellites: formation – protoplanetary discs – stars: formation –

## 1 INTRODUCTION

The population of young stellar objects known as transition discs have unusual spectral energy distributions (SEDs) that suggest that some portion of the inner disc has become optically thin (Strom et al. 1989; Skrutskie et al. 1990). The radial distribution of the dust disc has been inferred from detailed modeling of the SEDs, which have significant excesses beyond  $10\mu\text{m}$ , like those of normal T Tauri stars, but weak excesses at mid-infrared wavelengths (e.g., D’Alessio et al. 2005; Calvet et al. 2005). The optically thin region inferred from the modeling—a central “hole” in the dust distribution or an annular “gap” within a radius  $r_h$  of 15 AU to  $> 50$  AU depending on the source—has been confirmed by submillimeter interferometric imaging of bright, nearby systems (Andrews et al. 2011). These properties suggest that transition discs are in the process of dispersing their discs (see Espaillat et al. 2014 for a review).

Several scenarios have been proposed to explain the properties of transition discs. An early suggestion was that grain growth and planetesimal formation, the first steps toward planet formation via core accretion, might reduce the optical depth of the inner disc by reducing the dust cross-sectional area (Strom et al. 1989; see also Dullemond & Dominik 2005; Tanaka et al. 2005). The formation of giant

planets is also expected to carve a gap or inner cavity in the disc, rendering some or all of the inner disc optically thin (Skrutskie et al. 1990; Marsh & Mahoney 1992; Lubow et al. 1999; Calvet et al. 2002; Rice et al. 2003; Quillen et al. 2004; Calvet et al. 2005, D’Alessio et al. 2005; Rice et al. 2006). Alternatively, a photoevaporative wind, launched by the irradiation of the disc surface by stellar UV and X-rays, may also deplete the inner disc, by limiting the ability of material accreting from the outer disc to resupply the material in the inner disc (Clarke et al. 2001; Alexander et al. 2006; Alexander & Armitage 2007; Owen et al. 2010, 2011; Gorti et al. 2009). These interpretations are not mutually exclusive. For example, photoevaporation may disperse a disc more rapidly once a gap forms as a result of giant planet formation (e.g., Rosotti et al. 2013). Transition discs may also be produced through multiple pathways, with different processes potentially dominating on different timescales (e.g., Williams & Cieza 2011).

Because multiple processes can produce transition disc SEDs, other information (beyond SEDs) has been used in efforts to distinguish among the potential explanations. Detailed studies of individual transition discs have reported evidence for an orbiting companion (e.g., Kraus & Ireland 2012; Huelamo et al. 2011) or its circumplanetary disc (Brittain et al. 2013, 2014). Other studies have probed the spatial and velocity distribution of disc gas to look for evidence of photoevaporative outflows (e.g., Pascucci & Sterzik 2009;

\* E-mail: najita@noao.edu (JRN)

Sacco et al. 2012) or the radial truncation of the gaseous disc (e.g., Najita et al. 2008; Dutrey et al. 2008). The latter is not expected in the planetesimal scenario.

An alternative way to distinguish among the possible scenarios is to compare the demographic properties of populations of transition discs with those of normal (non-transition) T Tauri stars. Whereas recent studies have employed stellar accretion rates alone or in combination with properties such as X-ray luminosity and stellar mass for this purpose (Kim et al. 2009, 2013; Espaillat et al. 2012; Fang et al. 2013; Manara et al. 2014), the combination of stellar accretion rates and disc masses has also been suggested as a potentially powerful way to distinguish among the scenarios described above (Najita et al. 2007; Alexander & Armitage 2007; see also Cieza et al. 2008, 2010, 2012; Mendigutía et al. 2012). To summarize the basic idea:

(a) In the grain and planetesimal growth scenario, the dust component of the disc within  $r_h$  is altered but not the gas; the stellar accretion rate is therefore expected to be similar to that of normal T Tauri stars. Because planet formation is a common outcome of disc evolution (e.g., Fressin et al. 2013; Dong & Zhu 2013; Petigura et al. 2013), and planetesimal formation is the first step toward planet formation via core accretion, planetesimals are expected to form in discs of all masses.

(b) In contrast, when a forming Jovian-mass planet clears a gap in the disc, most of the accretion flow from the outer disc accretes onto the planet (in streams), and the stellar accretion rate is reduced to  $\sim 0.1$  of its original T Tauri value (Lubow et al. 1999; but see also Zhu et al. 2011). Because a Jovian-mass planet represents a significant mass reservoir relative to the median T Tauri disc mass (Andrews et al. 2013), planets massive enough to open a gap (e.g.,  $\gtrsim 1M_J$ ) are expected to form in discs with higher than average masses.

(c) The accreting planet could eventually reach a mass high enough ( $\sim 5M_J$ ) to suppress flow past the planet. When the remaining inner disc material accretes on to the star, an inner cavity in the gas and dust distribution of the disc would remain, with no further stellar accretion (e.g., Lubow et al. 1999; Lubow & D’Angelo 2006). Forming such high mass planets is favored in higher mass discs.

(d) If a photoevaporative wind can remove material from the disc faster than it can be replenished by accretion, the inner disc is starved of gas and dust, and stellar accretion drops to a low or negligible rate. This situation is more readily achieved in low mass discs (all other factors being equal; e.g., stellar irradiation fields) with initially modest accretion rates (e.g., Clarke et al. 2001; Alexander & Armitage 2007; Owen et al. 2010).

A previous study of stellar accretion rates and disc masses found evidence for a modest trend between stellar accretion rate and disc mass among single, normal T Tauri stars in Taurus (Najita et al. 2007). In addition, the Taurus transition discs were found to have disc masses  $\sim 4$  times larger than the normal T Tauri stars and stellar accretion rates  $\sim 10$  times lower than those of normal T Tauri stars of the same disc mass. These properties are most consistent with the interpretation that the Taurus transition discs are forming Jovian mass planets.

Here we extend the Taurus study by examining the stellar accretion rates  $\dot{M}_*$  and disc masses  $M_d$  of transition discs

and T Tauri stars in Ophiuchus in combination with the earlier Taurus results. Ophiuchus is one of the few star forming regions in which disc masses are available for a significant number of young stellar objects. Our study differs in several ways from the approach taken by Najita et al. (2007). The transition disc sample studied here is restricted to sources with evidence for large inner holes, i.e., sources with either a large MIR dip in the SED or a resolved cavity in submillimeter imaging of the source. Because of the large range of stellar spectral types in the Ophiuchus sample, we also correct for the dependence of stellar accretion rate on stellar mass. Our data sets are described in §2 and our analysis and results in §3. In §4, we discuss the location of transition discs in the  $\dot{M}_*-M_d$  plane and compare our results to those of previous studies. Our conclusions are summarized in §5.

## 2 DISK MASSES AND STELLAR ACCRETION RATES

For both the Taurus (Tau) and Ophiuchus (Oph) samples, we use stellar accretion rates and disc masses from the literature, with a few emendations as described below. Because we intend to compare the results for Oph with those previously obtained for Tau, the disc masses and stellar accretion rates for the two samples are treated as similarly as possible.

Millimeter continuum fluxes have been reported previously for many Oph sources. To incorporate these measurements in a homogeneous way in deriving disc masses, we follow the approach of Andrews et al. (2013) in their analysis of Tau disc masses. For each disc, we compiled and fit, using a power law model, all the available continuum measurements in the literature at wavelengths from  $700\mu\text{m}$  to  $3\text{mm}$  (Andre & Montmerle 1994; Dent et al. 1998; Nuernberger et al. 1998; Motte et al. 1998; Stanke et al. 2006; Andrews & Williams 2007a, b; Patience et al. 2008; Andrews et al. 2009, 2010; Ricci et al. 2010). These model fits and their associated uncertainties were extrapolated to estimate a flux density at a fiducial wavelength of  $1.33\text{mm}$ . If there was only 1 datapoint available in this range, we applied a mean power-law scaling to estimate the  $1.33\text{mm}$  flux density, where  $F_\nu \propto \nu^{2.5 \pm 0.4}$ .

We then calculated disc masses assuming the standard optically thin, isothermal approach, i.e.,

$$M_{d,\text{thin}} = \frac{d^2 F_\nu}{\kappa_\nu B_\nu(T_d)}, \quad (1)$$

for a fixed distance  $d$  ( $125\text{pc}$  for Oph,  $140\text{pc}$  for Tau) and opacity ( $\kappa_{1.33\text{mm}}(\text{dust}) = 2.3\text{cm}^2/\text{g}$ ; dust-to-gas ratio =  $0.01$ ). In these calculations, the average dust temperature for each source was computed from a simple estimate of the incident irradiation field, such that  $T_d = 25\text{K}(L_*/L_\odot)^{1/4}$ . This approximation assumes that the dust in discs is located at a common effective orbital distance, which is a reasonable assumption when spatially resolved information is unavailable (see Andrews et al. 2013 for details).

For Tau, we adopted the disc masses tabulated by Andrews et al. (2013) using the above method. For Oph, we determined  $M_{d,\text{thin}}$  using stellar luminosities from McClure et al. (2010). For both the Tau and Oph samples, we also investigated the impact of adopting  $M_d$  values estimated from fitting the SED and resolved millimeter imaging data

$M_{d,fit}$ . These are available for the brighter Tau and Oph sources (Andrews & Williams 2007b; Andrews et al. 2009, 2010, 2011).

The primary source of Oph stellar accretion rates is the large sample reported by Natta et al. (2006). Because of the high extinction toward  $\rho$ Oph, Natta et al. determined accretion rates from the IR hydrogen lines (Pa $\beta$  or Br $\gamma$ ) using the calibration of Muzerolle et al. (1998) to convert the IR line luminosities to accretion luminosities. For consistency with the adopted Oph disc masses, which involve a correction for  $L_*$ , we rederived the stellar accretion rate for each Oph source from the Pa $\beta$  equivalent width and  $J$ -band magnitude reported by Natta et al. (2006) using the extinction and  $L_*$  from McClure et al. (2010). The stellar masses used in the accretion rate determination were derived from the Siess et al. (2000) stellar evolutionary models using the approach and assumptions adopted by Andrews et al. (2013).

A few additional Oph accretion rates were adopted from Espaillat et al. (2010), Eisner et al. (2005), and Valenti et al. (1993). The accretion rate determined by Espaillat et al. (2010) for DoAr44 (also known as ROXs-44) was derived from the  $U$ -band excess reported by Bouvier & Appenzeller (1992) following the Gullbring et al. (1998) method (Andrews et al. 2011; C. Espaillat 2013, personal communication). Eisner et al. (2005) report an accretion rate for WaOph6 (V2508 Oph) that is based on a  $U$ -band excess derived from  $UBVRI$  photometry and high resolution optical spectroscopy following the method of Gullbring et al. (1998). Because the Muzerolle et al. (1998) relations used by Natta et al. (2006) were originally calibrated with accretion rates derived via the Gullbring method, the set of  $\dot{M}_*$  values used here should be on a consistent footing. The properties of the Oph sample are shown in Table 1.

For the Tau sample, we adopted stellar accretion rates from Najita et al. (2007) and also included a few additional stellar accretion rates from Valenti et al. (1993; GI Tau, HN Tau) and Hartigan et al. (1995; HK Tau). As in Najita et al. (2007), the values from Hartigan et al. (1995) were scaled downward by a factor of 0.17 for consistency with the stellar accretion rates of Hartmann et al. (1998).<sup>1</sup> In order to investigate the impact of the known trend between  $\dot{M}_*$  and  $M_*$ , we also adopted the stellar masses reported by Andrews et al. (2013) using the Siess et al. (2000) models. The properties of the single star Tau sample are shown in Table 2.

The Oph sample includes both sources in the  $\sim 2$  Myr old surface population and the surrounding region (Wilking et al. 2005) as well as the younger embedded sources in the Oph core ( $< 1$  Myr; Luhman & Rieke 1999). In comparison, Tau has a median age of  $\sim 2$  Myr with a distribution between 1 Myr and a few Myr (Kenyon & Hartmann 1995; Hartmann 2001; Luhman et al. 2003; Andrews et al. 2013).

### 3 RESULTS

Despite the large samples of Oph stellar accretion rates and disc mass estimates reported by Natta et al. (2006) and

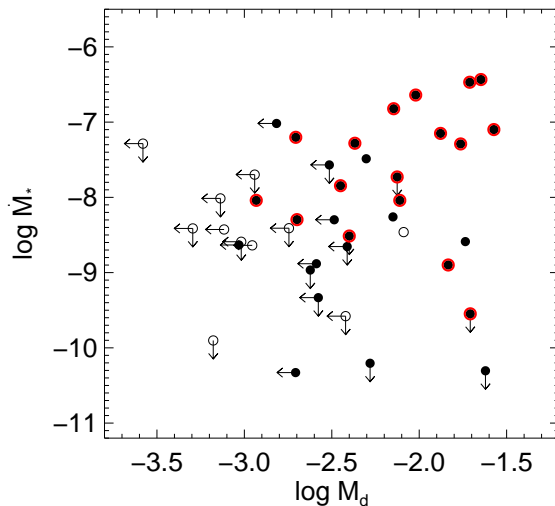


**Figure 1.** Stellar accretion rates (in  $M_\odot \text{ yr}^{-1}$ ) and disc masses (in  $M_\odot$ ) for Ophiuchus sources. Arrows indicate upper limits. Closed (open) circles designate sources without (with) known companions within  $1''$ . Binaries have lower disc masses than single stars. Sources with spectral types earlier than M0 (symbols with a red rim) have higher average stellar accretion rates than sources with later spectral types.

Andrews & Williams (2007a) ( $\sim 140$  sources in each) the overlap between the two samples is limited ( $\sim 40$  sources). The limited overlap is partly due to different areal coverage. Natta et al. (2006) studied the Oph core, whereas Andrews & Williams (2007a) studied a larger area. In addition, both samples include a significant fraction of sources that are either Class III or Class I (25%–35%). Figure 1 shows sources that have detections or upper limits (indicated by arrows) for both quantities. Sources with a known stellar companion within  $1''$  (Reipurth & Zinnecker 1993; Barsony et al. 2005; Ratzka et al. 2005) are shown as open circles. Sources without such a companion are regarded as single stars (solid symbols). The binaries have lower average disc masses than the single stars, consistent with similar trends noted elsewhere in the literature (e.g., Jensen et al. 1994, 1996; Andrews & Williams 2005; Harris et al. 2012). The presence of a stellar companion is believed to dynamically alter the structure of the disc, reducing its mass. We therefore excluded the binaries from further consideration.

In Figure 1, sources with later spectral types (later than M1) have lower average  $\dot{M}_*$  than earlier types, a result that is not surprising given the well-known trend of increasing  $\dot{M}_*$  with  $M_*$  (e.g., Muzerolle et al. 2003; Calvet et al. 2004; Natta et al. 2006; Fang et al. 2009; Rigliaco et al. 2011; Manara et al. 2012). This trend was not an issue in the earlier Taurus study, because the Tau sample spans a more limited range of spectral types (K2–M2;  $\sim 80\%$  are K3–M0 or  $\sim 0.5 - 1.5 M_\odot$ ). Because the trend of  $\dot{M}_*$  with  $M_*$  has a large scatter at  $\sim 1$  Myr age ( $\sim 2$  orders of magnitude at a given  $M_*$ ; e.g., Fang et al. 2013), the trend is only apparent over a mass range of  $\gtrsim 1$  dex (e.g., Muzerolle et al. 2003; Manara et al. 2012), as in our Oph sample (A1–M6;  $\sim 0.07 - 4 M_\odot$ ).

We therefore corrected the Oph sample for the trend

<sup>1</sup> In Najita et al. (2007) we also scaled the stellar accretion rates of White & Ghez (2001) up by 2.4.

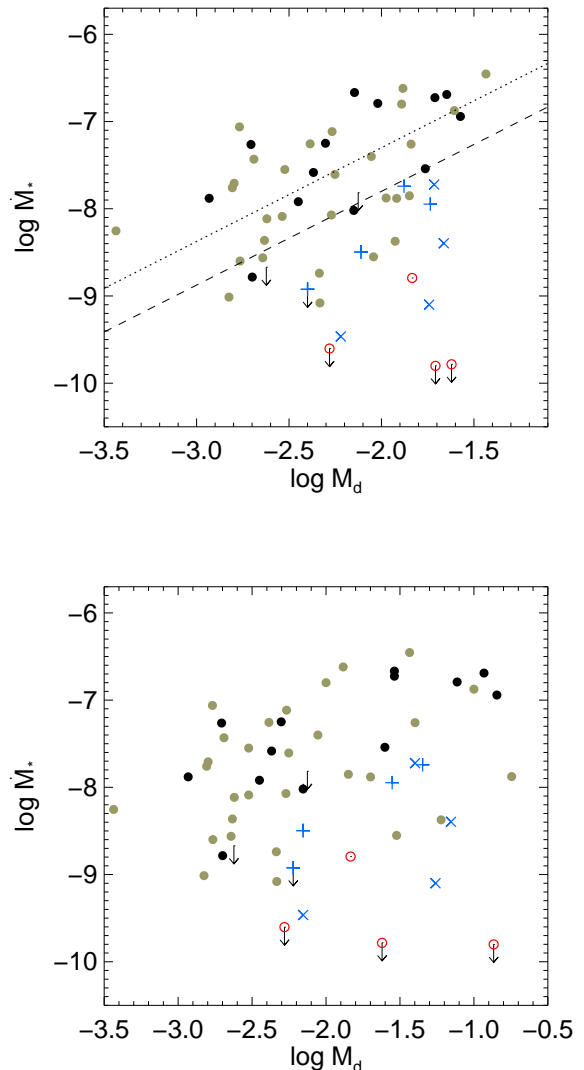
between  $\dot{M}_*$  and  $M_*$  in order to include its larger range of spectral types and maximize its sample size. The derived Oph accretion rates  $\dot{M}_{*0}$  were rescaled as  $\log \dot{M}_{*,\text{norm}} = \log \dot{M}_{*0} - 1.3 \log(M_*/0.7M_\odot)$  using the slope from Manara et al. (2012) for a 1 Myr population and our estimated stellar masses (section 2). In exploring alternative approaches, we found that the effect of the rescaling on our results is insensitive to the details of which stellar evolutionary tracks are used in estimating stellar masses or whether the appropriate relation has a steeper slope (e.g.,  $\dot{M}_* \propto M_*^2$  as in Muzerolle et al. 2003). We also explored but did not adopt a correction for a possible trend of  $M_d \propto M_*$  (Andrews et al. 2013), because it did not affect our results. This is understandable because  $M_d$  and  $M_*$  are not strongly correlated over the primary mass range of our sample ( $\log M_* = -0.65$  to 0.3; Andrews et al. 2013).

Figure 2a shows the rescaled Oph accretion rates plotted against  $M_{d,\text{thin}}$  (black dots) where, for clarity, sources with upper limits on their disc mass are not shown. Sources with a transition disc SED and/or a submillimeter cavity (Espaillat et al. 2010, McClure et al. 2010; Andrews et al. 2011) are indicated by blue ‘+’ symbols. Single T Tauri stars (gray dots) and transition discs (blue ‘x’ symbols) in Taurus are also shown (see Najita et al. 2007 and section 2), where we have applied the same rescaling of  $\dot{M}_*$  as a function of  $M_*$  that was used for the Oph sample. The Oph transition discs fall between the regions occupied by the Tau transition discs and the normal T Tauri stars.

Most of the sources marked as transition discs in Table 1 and Figure 2 have prominent mid-infrared (MIR) dips in their SEDs. Because there are only 2 such Oph objects with  $\dot{M}_*$  measurements (SR21A, DoAr44; McClure et al. 2010), we also included Oph sources that have a submillimeter cavity (but lack a MIR SED dip) for which  $\dot{M}_*$  is available (SR24S, WSB60; Andrews et al. 2011). These sources (both with and without MIR SED dips) have submillimeter cavity radii of 15–36 AU (Andrews et al. 2011). Because submillimeter imaging studies have been limited to the brighter sources ( $> 75$  mJy at  $880\mu\text{m}$  or  $M_d \gtrsim 0.005M_\odot$  for the Oph SMA sample; Andrews et al. 2010), the sample of cavity sources may be artificially biased to higher disk masses; i.e., lower mass disks may possess cavities that have not yet been identified. In contrast, selecting transition discs by their prominent MIR SED dip should not introduce a similar bias. For example, a system like CoKu Tau/4, which has a prominent MIR SED dip, has a very low disk mass ( $\sim 0.001M_\odot$ ; D’Alessio et al. 2005).

The Tau transition disc sample differs from that of Najita et al. (2007), who defined transition discs more broadly based on weak or no excess shortward of  $10\mu\text{m}$  and a significant excess at longer wavelengths. Because such a broad definition is debated, we have adopted a more conservative definition here by selecting only objects with prominent MIR dips in their SEDs (DM Tau, GM Aur, UX Tau, LkCa15; Calvet et al. 2005; Espaillat et al. 2010). The remaining sources in the Tau sample are classified as normal T Tauri stars.

To explore the impact of our simple prescription for disc mass (eq. 1), Figure 2b shows the same information except that the Tau and Oph disc masses estimated from radiative transfer models that simultaneously fit SEDs and resolved millimeter-wavelength visibilities  $M_{d,\text{fit}}$  are used when avail-



**Figure 2.** Top (a): Stellar accretion rates (in  $M_\odot \text{yr}^{-1}$ ) and disc masses (in  $M_\odot$ ) of T Tauri stars in Ophiuchus (black dots) and Taurus (gray dots) compared with transition discs in Ophiuchus (blue ‘+’) and Taurus (blue ‘x’). Red circles indicate the Ophiuchus outlier population, i.e., T Tauri stars with normal SEDs that have very low accretion rates for their disc masses. For clarity, only non-binaries and sources with  $M_d$  detections are shown. Stellar accretion rates have been adjusted for the known dependence of  $\dot{M}_*$  on  $M_*$ . Arrows indicate sources with upper limits on their stellar accretion rates. The dotted line is a linear fit to the normal T Tauri stars; the dashed line, located  $1-\sigma$  below the dotted line, divides the plane into two regions (see text for details). Bottom (b): Similar to the top panel except that disc mass estimates from fits to resolved millimeter-wavelength visibilities  $M_{d,\text{fit}}$  are used when available. In either plot, transition discs have lower than average accretion rates for their disc mass.

able (Andrews & Williams 2007b; Andrews et al. 2009, 2010, 2011). Of the 13 Oph sources with  $M_{d,\text{fit}}$  values, roughly half have  $M_{d,\text{fit}}$  values within 60% of the  $M_{d,\text{thin}}$  value. The other half have  $M_{d,\text{fit}}$  values  $\sim 5$  times larger. The large difference for sources such as WaOph6 and DoAr25 occurs because the dust associated with these sources is colder and the disc is

larger in size than one would infer from the simple optically thin scaling used for  $M_{d,\text{thin}}$ . A similar result is found for the Tau sources.

Note that the Tau accretion rates and disc masses shown in Figure 2a differ from those adopted in Najita et al. (2007). Here the accretion rates are scaled by  $M_*$ , and the optically thin disc masses assume a common effective orbital distance rather than a common average temperature for the emitting dust grains. That is, the characteristic (mass-weighted) temperature of the emitting grains, when averaged over the radial structure of the disc, depends on  $L_*$ ; in contrast, the Andrews & Williams (2005) disc masses used in Najita et al. (2007) assumed a characteristic grain temperature of 20 K for all sources (for details see section 3.2.2 of Andrews et al. 2013).

As shown in Figure 2, with either set of disc mass estimates, the normal (single) T Tauri stars in Oph overlap the region of the diagram occupied by the normal (single) T Tauri stars in Tau. Among the sources with measured stellar accretion rates and disc masses, there is a trend of  $\dot{M}_*$  increasing with  $M_d$ , albeit with significant dispersion. A similar result was noted previously for the Tau sample alone (Najita et al. 2007). A trend of  $\dot{M}_*$  increasing with  $M_d$  is not surprising; in  $\alpha$ -viscosity discs (e.g., Shakura & Sunyaev 1973) the accretion rate is proportional to the disc column density (or mass).

Time variability and measurement uncertainty in the stellar accretion rate likely account for some of the observed scatter about the mean trend. Stellar accretion rates of individual objects are known to vary by a factor of  $\sim 2$  (e.g., Hartigan et al. 1991). Gullbring et al. (1998) reported typical measurement uncertainties of 0.5 dex in their stellar accretion rates; Natta et al. (2006) did not report their uncertainties.

The assumptions made in deriving disc masses are also a likely source of dispersion. Disks may be partially optically thick or have different temperature distributions than assumed in the prescription of Andrews et al. (2013). In addition,  $M_d$  measurements are insensitive to solids that have grown into large grains ( $\gtrsim$  cm). Dispersion in the solid size distribution would mean dispersion in the extent to which the millimeter continuum traces the gas mass. Unrecognized binarity (and its impact on either or both of  $\dot{M}_*$  and  $M_d$ ) is yet another potential source of dispersion, although more so for Oph than for Tau. The binarity of the latter population is now fairly well known (e.g., Kraus et al. 2011).

Several additional Oph sources have low  $\dot{M}_*$  for their  $M_d$  but lack obvious MIR dips in their SED (Fig. 2, red open circles). DoAr 25, GY284, and WL14 have upper limits below  $\log \dot{M}_* = -9.5$ , and LFAM3 has the lowest Oph  $\log \dot{M}_*$  measurement in the plot. WL14 and LFAM3 have high estimated extinction values ( $A_v > 15$ ), with their stellar accretion rates possibly underestimated as a result. We discuss this issue and the possible nature of these ‘‘outlier’’ sources in the next section.

We also find that the known Oph transition discs occupy roughly the same region of the  $\dot{M}_*-M_d$  plane as the Tau transition discs. That is, the Oph transition discs have lower accretion rates for their disc masses than do normal T Tauri stars in Tau and Oph. In Figure 2a, the median  $\log \dot{M}_*$  for the normal T Tauri stars (outliers excluded) and transition discs is -7.6 and -8.4, respectively; the median  $\log M_d$

is -2.3 and -1.7, respectively. If the outliers were included in the normal T Tauri population, the median  $\log \dot{M}_*$  would decrease slightly to -7.8; the median  $\log M_d$  would be unchanged.

With the addition of the Oph sources, we can describe more quantitatively the trend between  $\log M_d$  and  $\log \dot{M}_*$  for the normal T Tauri population (outliers excluded) in Figure 2a. The Kendall  $\tau$  for the individual Tau and Oph and the combined (Tau+Oph) normal T Tauri samples is 0.34, 0.46, and 0.38, respectively, with corresponding 2-sided  $p$ -values of 0.96%, 2.8%, and 0.03%. The reduced  $p$ -value of the combined sample illustrates the value of the Oph sources in improving the statistical significance of the trend. Including the outliers in the normal T Tauri population reduces the Kendall  $\tau$  to 0.23 ( $p$ -value of 2.3%), consistent with the visual impression of these sources as outliers.

We estimated the slope of the trend using Brandon Kelly’s *linmix\_err\_idl* routine (Kelly 2007), which takes a Bayesian approach to linear regression given errors in both quantities. Assuming errors of 0.2 dex in  $\log M_{d,\text{thin}}$  and 0.3 dex in  $\log \dot{M}_{*,\text{norm}}$ , we find

$$\log \dot{M}_{*,\text{norm}} = -5.15(\pm 0.75) + 1.08(\pm 0.3) \log M_{d,\text{thin}} \quad (2)$$

with a dispersion about this trend of  $\sigma(\log \dot{M}_{*,\text{norm}}) = 0.5$ . If the Tau and Oph normal T Tauri star populations are examined separately, they have similar slopes ( $\sim 1$ ) and dispersion ( $\sim 0.5$  dex). The  $\dot{M}_{*,\text{norm}}$  normalization constant for the Oph normal T Tauri population is larger by 0.75 dex than that of the Tau population, consistent with the visual impression, although the uncertainty in the values of the constants is large.

The small sample size of the transition discs makes it difficult to compare in detail the distributions of the normal T Tauri stars and transition disc populations in the  $\log M_d$ - $\log \dot{M}_*$  plane. For example, if we were to fit a linear trend to the transition disc sample for comparison with the fit for the normal T Tauri stars (eq. 2), the uncertainty on the slope and constant would be too large for a meaningful comparison. However, we can explore whether the distributions of the two populations in the  $\dot{M}_*-M_d$  plane are grossly similar by dividing the plane into two regions and seeing whether there is a statistical difference in the distribution of the two populations across the two regions. Using the distribution of normal T Tauri stars as a guide, since it is the better characterized population, we divide the plane at a line located 1- $\sigma$  below the mean  $\log M_{d,\text{thin}}-\log \dot{M}_{*,\text{norm}}$  relation for the Tau+Oph normal T Tauri stars (eq. 2), i.e., at

$$\log \dot{M}_{*,\text{norm}} = -5.65 + 1.08 \log M_{d,\text{thin}} \quad (3)$$

(Fig. 2a, dashed line). As expected, many more of the normal T Tauri stars in the combined sample lie above the line (32 sources) than below the line (12 sources). In contrast, there are no transition discs above the line and 8 below. For the purpose of apportioning the sample, upper limits in  $\log \dot{M}_*$  are treated as detections, although the results are insensitive to how they are treated.

We can use a contingency table analysis (e.g., Busmann et al. 2011) to see whether these values are consistent with the null hypothesis that the populations are similarly distributed above and below the line. Fisher’s exact test, which is a useful approach when the sample sizes are small, gives a probability of 0 that the T Tauri stars and transition discs

are similarly distributed. The result is insensitive to where the boundary (eq. 3) is drawn. If the boundary were a factor of 2, 2.5, or 3 times higher in  $\log \dot{M}_*$ , the probability would still be only 0.002, 0.006, or 0.014 that the T Tauri stars and transition discs are similarly distributed. The boundary in the last case is coincident with the locus of the mean trend (Fig. 2a, dotted line). If the boundary were a factor of 2 or 3 lower in  $\log \dot{M}_*$ , the probability remains low at 0.001 or 0.002 respectively. Including the outliers in the normal T Tauri population raises the above probabilities slightly (by a factor of  $\sim 2$ ) but does not change our finding that the transition discs and normal T Tauri stars are not similarly distributed in the  $\dot{M}_*-M_d$  plane. As a contrasting example, we can also compare the distributions of the Tau and Oph normal T Tauri stars across the boundary (eq. 3). The probability that the two populations are similarly distributed is 21%.

## 4 DISCUSSION

As described in the previous section, when combined with the Tau sample, the Oph sample enhances the statistical significance of the previously reported trend of  $\dot{M}_*$  vs.  $M_d$  among single, normal T Tauri stars. The Oph transition discs, like the Tau transition discs, are found to favor the lower right region of the  $\dot{M}_*-M_d$  plane, i.e., transition discs tend to have lower  $\dot{M}_*$  for a given  $M_d$  and a higher  $M_d$  (for a given  $\dot{M}_*$ ) than normal T Tauri stars.

Planetesimal formation does not provide a ready explanation for this result. Naively, we would expect that systems forming planetesimals would have accretion rates similar to those of normal T Tauri stars, because planetesimal formation alters the size distribution of the disc solids, but it is not known to alter the properties of the disc gas and stellar accretion rate. While this result was obtained previously for the Tau transition disc sample, it also appears to apply at the younger average age of Oph, when planetesimal formation, as the first step in planet formation in the core accretion scenario, would be even more likely to dominate over the other proposed explanations for transition discs (giant planet formation, photoevaporation). The lack of transition discs meeting our expectations for where planetesimal-forming systems would lie in the  $\dot{M}_*-M_d$  plane, for both the Tau and Oph samples, argues against planetesimal formation as a significant pathway to form transition discs at the ages of nearby star forming regions (1 – 3 Myr).

This interpretation is consistent with the results of recent theoretical studies that find it difficult to replicate the properties of transition discs through grain evolution alone. Early models of grain evolution that considered sticking without fragmentation were able to produce MIR SED dips like those of transition discs (Dullemond & Dominik 2005; Tanaka et al. 2005). However, recent, more realistic grain evolution models that include coagulation, fragmentation, radial drift, gas drag, and turbulent mixing (Birnstiel et al. 2012) find that while discs can develop the MIR dips that characterize transition disc SEDs, enough non-fragmenting centimeter-sized particles remain behind that these systems would not show the submillimeter cavities that also characterize transition discs. A similar difficulty is found even under the simplified conditions considered in earlier models

(perfect sticking in the absence of radial draft; e.g., Dullemond & Dominik 2005).

The measurable  $M_*$  and higher average  $M_d$  of transition discs compared to normal T Tauri stars also suggests that photoevaporation is not the dominant pathway to a transition disc at Taurus-Ophiuchus age. Photoevaporation is more likely to create an inner cavity in the disc in systems with low  $\dot{M}_*$  and low  $M_d$ , if all other factors are equal (e.g., Alexander & Armitage 2007).

The low  $\dot{M}_*$  of transition discs for their disc masses relative to normal T Tauri stars is most consistent with the formation of objects massive enough to alter the disc accretion flow, i.e., giant planet formation. Interestingly, this is the case for both systems with transition disc SEDs and those with submillimeter cavities. Sources such as DoAr44, a transition disc with a prominent MIR SED dip, are hypothesized to have formed giant planetary companion(s) (e.g., Espaillat et al. 2010).

Why do we find low accretion rates for transition discs both with and without MIR dips in their SEDs? Perhaps the conditions needed to reduce the stellar accretion rate are less stringent than those needed to render the inner disc optically thin in the MIR. Removing small dust grains from the inner disc enough to render it optically thin while also allowing continued accretion onto the star is a recognized challenge (Rice et al. 2006; Zhu et al. 2012). Whether a system with a submillimeter cavity also develops an optically thin inner disc in the MIR (i.e., a transition disc SED) may therefore require the formation of higher mass companions and/or a larger number of companions (Zhu et al. 2011; Dodson-Robinson & Salyk 2011). For example, a more massive companion or more of them may induce a larger pressure bump at the inner edge of the outer disc, enhancing the efficiency of dust filtering (Rice et al. 2006). Radiation pressure from a high mass accreting planet can also play a role in creating a transition disc SED (Owen 2014). In comparison, the formation of a single, low mass giant planet may be sufficient to create a submillimeter cavity and to impact the disc accretion rate (e.g., Lubow et al. 1999).

In §3, we noted a few outliers among the Oph sources in the  $\dot{M}_*-M_d$  plot, i.e., sources with normal T Tauri SEDs but low accretion rates for their disc mass. For some sources, their high  $A_V$  may have led to an underestimate of their accretion rates (WL14, LFAM3). In sources with very high reddening, such as highly-inclined discs or protostars, the scattered light component can dominate the observed light into the near-infrared. Because the colors then appear bluer than would be produced by the extinction along the line of sight to the central source, the typical methods of determining the extinction using observed near-infrared colors and assuming an intrinsic color from a known spectral type or the classical T Tauri star locus will underestimate the extinction. Subsequent dereddening of the observed line flux will lead to an underestimate of the true line luminosity, and by extension,  $\dot{M}_*$ . Correcting for this effect for a given source depends on the scattering fraction, which is difficult to determine.

Another possibility is that some or all of the low accretion rate sources may be unrecognized transition discs in which giant planet formation either (i) has occurred at disc radii too small to probe with SEDs or submillimeter imaging or (ii) is insufficiently advanced (e.g., the planet is too low

in mass or too few in number) to render portions of the disc optically thin. This scenario may be particularly relevant to the two outliers that have only modest extinction (DoAr25 at  $A_v = 3.4$  and GY284 at  $A_v = 6$ ).

Andrews et al. (2008) previously noted that DoAr25 has a low stellar accretion rate for its disc mass. Although DoAr25 has one of the highest measured disc masses ( $0.14M_\odot$ ), stellar accretion estimates range from  $< 2 \times 10^{-10}M_\odot \text{ yr}^{-1}$  (Natta et al. 2006) to  $3 \times 10^{-9}M_\odot \text{ yr}^{-1}$  (Greene & Lada 1996; Luhman & Rieke 1999). Transition discs like LkCa15 and UX TauA, which also have low accretion rates for their disc masses, have such large gaps ( $\gtrsim 25$  AU) that multiple giant planets, spread out over a range of radii, have been invoked to explain the large optically thin regions (Zhu et al. 2011). In contrast, T Tauri discs that have formed a single giant planet are expected to clear much smaller gaps, particularly if the planet is located at small disc radii, e.g., at a Jupiter-like distance of 5 AU. A high mass giant planet ( $\sim 5M_J$ ) located at such a distance is expected to greatly reduce the stellar accretion rate (Lubow et al. 1999). Given its large disc mass ( $\sim 0.1M_\odot$ ), it seems possible that DoAr25 may have formed such a giant planet. Interestingly, the accretion rate estimates in the literature for DoAr25 differ by more than a factor of 10. Extreme variability (by such a large factor) in the stellar accretion rate is unusual (e.g., Nguyen et al. 2009) and may be consistent with the presence of a massive close companion (e.g., Basri et al. 1997).

Other sources near Oph may share these properties. For example, the MIR colors of RXJ1633.9-2242 (source #32 in Cieza et al. 2010) are consistent with the presence of a disk cavity  $\sim 8$  AU in radius (Orellana et al. 2012). The source has a fairly large disk mass ( $M_d \simeq 0.01\text{--}0.02M_\odot$ ) and a low estimated accretion rate based on its H $\alpha$  width ( $\dot{M}_* = 10^{-10}M_\odot \text{ yr}^{-1}$ ). The low accretion rate could be confirmed with a more accurate accretion rate diagnostic (e.g., IR hydrogen line luminosities or  $U$ -band excess).

Cavities 5 AU or 8 AU in radius would have been difficult to detect in the submillimeter studies of nearby young stars reported to date. The smallest dust cavity reported in the SMA study of Andrews et al. (2011) has a radius of 15 AU (WSB60). Higher angular resolution observations (e.g., with ALMA) of DoAr25 and the other low accretion rate systems would explore whether these systems are like the known Oph transition discs in having inner cavities.

Thus we find that the combination of stellar accretion rates and disc masses can help to distinguish among proposed scenarios for the origin of transition discs. Toward this end, we have attempted to control for the known dependencies of  $\dot{M}_*$  and  $M_d$  on age (e.g., Hartmann et al. 1998),  $\dot{M}_*$  on stellar mass (e.g., Muzerolle et al. 2003), and  $M_d$  on the presence of stellar or sub-stellar companions (e.g., Artymowicz & Lubow 1996; Lubow et al. 1999) by (i) comparing the properties of transition discs and normal T Tauri stars in the same star-forming region, (ii) correcting for the known dependence of  $\dot{M}_*$  on  $M_*$ , and (iii) excluding known binaries, respectively. With this approach, we find that including disc masses in the demographic analysis helps to accentuate decrements in the stellar accretion rates of transition disc subpopulations relative to normal T Tauri stars.

Our results complement previous studies that have taken different approaches in examining the accretion rates

of transition discs in other star forming regions. Some of the earlier studies focused on sources older than those studied here. For example, in the Tr 37 and NGC 7160 clusters in Cep OB2 ( $\sim 4$  Myr and  $\sim 12$  Myr respectively), half the transition discs exhibit no measurable accretion, and the accretion rates of the other half are similar to those of classical T Tauri stars in the region ( $2 - 3 \times 10^{-9}M_\odot \text{ yr}^{-1}$ ; Sicilia-Aguilar et al. 2010). These results may differ from our result because the dominant physical mechanism that produces transition disc SEDs may differ between ages of 1 Myr and 10 Myr; e.g., photoevaporation may dominate at late times.

Several studies have compared the stellar accretion rates (but not disc masses) of transition discs and T Tauri stars in star forming regions similar in age to those studied here ( $\lesssim 3$  Myr). Similar in spirit to our results, some studies have reported evidence that transition discs have lower accretion rates (Espaillat et al. 2012) or lower accretion luminosities (Salyk et al. 2013) than normal T Tauri stars. Kim et al. (2013) found that transition discs in Orion A have accretion rates a factor of  $\sim 10$  lower, on average, than Taurus T Tauri stars of the same stellar mass. In contrast, Fang et al. (2013) found that accreting transition discs in L1641 have a median accretion rate (from H $\alpha$ ) similar to that of the T Tauri stars in the region. However, their transition disc accretion rates determined from H $\beta$  luminosity do have a lower median value (by a factor  $\sim 3$ ) than T Tauri stars of the same stellar mass. H $\beta$  luminosity may more reliably trace accretion rate than H $\alpha$ , because H $\alpha$  is more optically thick and it can be reduced in strength by wind absorption components (e.g., Muzerolle et al. 1998).

The choice of comparison samples may also play a role in the the interpretation of accretion rates. Manara et al. (2014) compared the accretion rates of transition discs in a variety of star forming regions (Taurus, Ophiuchus, Chamaeleon, Serpens) with the accretion rates of T Tauri stars in Lupus I and II. The transition discs appear biased toward lower  $\dot{M}_*$ , with a median  $\dot{M}_* \sim 3$  times lower than the average rate for the T Tauri stars for the same  $M_*$ . The use of Lupus T Tauri stars as the comparison sample may underestimate the  $\dot{M}_*$  decrement, because stellar accretion rate declines with age (Hartmann et al. 1998), and the Lupus I and II regions ( $\sim 3$  Myr; Alcalá et al. 2014) may be older than most of the transition discs in the Manara et al. study (1–2 Myr for Tau, Oph, Cha; e.g., Furlan et al. 2009). The average  $\dot{M}_*$  for Lupus T Tauri stars ( $0.4\text{--}0.8M_\odot$ ) is  $1.3 \times 10^{-9}M_\odot \text{ yr}^{-1}$  (Alcalá et al. 2014), whereas the mean  $\dot{M}_*$  for Taurus T Tauri stars is  $\sim 10^{-8}M_\odot \text{ yr}^{-1}$  (Hartmann et al. 1998). Thus, other studies in the literature appear to find results consistent with those reported here when we consider the accretion rate tracers and comparison populations used.

## 5 SUMMARY AND CONCLUSIONS

We find that the combination of stellar accretion rates and disc masses can aid in distinguishing among proposed explanations for the unusual SEDs of the population of young stellar objects known as transition discs. Determining how stellar accretion rate depends on a parameter such as SED shape can be a challenge because accretion rate is known to



depend on other parameters such as age (e.g., Hartmann et al. 1998), stellar mass (e.g., Muzerolle et al. 2003), disc mass (Najita et al. 2007), and potentially the presence of stellar or sub-stellar companions (e.g., Artymowicz & Lubow 1996; Lubow et al. 1999). In our study, we have attempted to control for these known dependencies by (i) comparing the properties of transition discs and normal T Tauri stars in the same star-forming region, (ii) correcting for the known dependence of  $\dot{M}_*$  on  $M_*$ , (iii) using available  $M_d$  measurements, and (iv) excluding known binaries, respectively.

Using this approach, we compared the distributions in the  $\dot{M}_*-M_d$  plane of transition discs and single, normal T Tauri stars in Taurus and Ophiuchus. The transition discs we studied have prominent MIR dips in their *Spitzer* SEDs or inner cavities in submillimeter continuum images. The available data suggest some interesting trends:

1. When combined with the Tau sample, the Oph sample enhances the statistical significance of the previously reported trend of  $\dot{M}_*$  vs.  $M_d$  among single, normal T Tauri stars.

2. The Tau and Oph transition discs we studied favor the lower right region of the  $\dot{M}_*-M_d$  plane, i.e., they tend to have lower  $\dot{M}_*$  for a given  $M_d$  and a higher  $M_d$  (for a given  $\dot{M}_*$ ) than normal T Tauri stars. This result is most consistent with the formation of objects massive enough to alter the accretion flow, i.e., single or multiple giant planets.

3. Several T Tauri stars that are not known transition disc systems also have low accretion rates for their disc masses. Such sources that also have high extinctions may have underestimated stellar accretion rates (LFAM3, WL14). The others may have formed (high mass) giant planets that are massive enough to greatly reduce the stellar accretion rate, but the planets are located at orbital radii too small to have an observable impact on the submillimeter continuum image or a distinctive impact on the SED (DoAr25, GY284). More detailed studies of the extinction toward these sources, their stellar accretion rates, and disc structure would help to distinguish between these possibilities.

## ACKNOWLEDGMENTS

We are grateful to Melissa McClure for providing the stellar luminosities for the Oph sources studied here. JN is grateful to the Institute for Theory and Computation at the Harvard-Smithsonian Center for Astrophysics for supporting a sabbatical visit that enabled this study.

## REFERENCES

Alcalá, J. M., et al., 2014, *A&A*, 561, 2  
 Alexander R. D., Clarke C. J., Pringle J. E., 2006, *MNRAS*, 369, 229  
 Alexander R. D., Armitage, P. J., 2007, *MNRAS*, 375, 500  
 André, P., Montmerle, T., 1994, *ApJ*, 420, 837  
 Andrews S. M., Rosenfeld, K. A., Kraus, A. L., Wilner, D. J., 2013, *ApJ*, 771, 129  
 Andrews S. M., et al. 2011, *ApJ*, 732, 42  
 Andrews S. M., Wilner, D. J., Hughes, A. M., Qi, C., Dullemond, C. P., 2010, *ApJ*, 723, 1241

Andrews S. M., Wilner, D. J., Hughes, A. M., Qi, C., Dullemond, C. P., 2009, *ApJ*, 700, 1502  
 Andrews, S. M., Hughes, A. M., Wilner, D. J., Qi, C., 2008, *ApJ*, 678, L133  
 Andrews S. M., Williams J. P., 2007a, *ApJ*, 671, 1800  
 Andrews S. M., Williams J. P., 2007b, *ApJ*, 659, 705  
 Andrews S. M., Williams J. P., 2005, *ApJ*, 631, 1134  
 Artymowicz, P., Lubow, S. H., 1996, *ApJ*, 467, L77  
 Barsony, M., Ressler, M. E., Marsh, K. A., 2005, *ApJ*, 630, 381  
 Birnstiel T., Andrews S. M., Ercolano B., 2012, *A&A*, 544, A79  
 Bouvier, J., Appenzeller, I., 1992, *A&AS*, 92, 481  
 Brittain, S. D., Najita, J. R., Carr, J. S., Liskowsky, J., Troutman, M. R., Doppmann, G. W., 2013, *ApJ*, 767, 159  
 Brittain, S. D., Carr, J. S., Najita, J. R., Quanz, S. P., Meyer, M. R., 2014, *ApJ*, 791, 136  
 Bussmann, R. S., et al., 2011, *ApJ*, 733, 21  
 Calvet N. et al., 2005, *ApJ*, 630, L185  
 Calvet N., D'Alessio P., Hartmann L., Wilner D., Walsh A., Sitko M., 2002, *ApJ*, 568, 1008  
 Calvet N., Muzerolle J., Briceño C., Hernandez J., Hartmann L., Saucedo J. L., Gordon K. D., 2004, *AJ*, 128, 1294 (C04)  
 Cieza, L. A., Swift, J. J., Mathews, G. S., Williams, J. P., 2008, *ApJ*, 686, L115  
 Cieza, L. A., et al., 2010, *ApJ*, 712, 925  
 Cieza, L. A., Schreiber, M. R., Romero, G. A., Williams, J. P., Rebassa-Mansergas, A., Merín, B., 2012, *ApJ*, 750, 157  
 Clarke C. J., Gendrin A., Sotomayor M., 2001, *MNRAS*, 328, 485  
 Cushing, M. C., Tokunaga, A. T., Kobayashi, N., 2000, *AJ*, 119, 3019  
 D'Alessio P. et al., 2005, *ApJ*, 621, 461  
 Dent, W. R., F., Matthews, H. E., Ward-Thompson, D., 1998, *MNRAS*, 301, 1049  
 Dodson-Robinson, S. E., Salyk, C., 2011, *ApJ*, 738, 131  
 Dong, S., Zhu, Z., 2013, *ApJ*, 778, 53  
 Dullemond C. P., Dominik C., 2005, *A&A*, 434, 971  
 Dutrey, A. et al., 2008, *A&A*, 490, L15  
 Eisner, J. et al. 2005  
 Espaillat, C., et al., 2010, *ApJ*, 717, 441  
 Espaillat C. et al., 2014, in *Protostars and Planets VI*, Beuther H., Klessen R. S., Dullemond C. P., Henning T., eds, Univ. Arizona, Tucson, p. 497  
 Espaillat, C., et al., 2012, *ApJ*, 747, 103  
 Fang, M., Kim, J. S., van Boekel, R., Sicilia-Aguilar, A., Henning, T., Flaherty, K., 2013, *ApJS*, 207, 5  
 Fang, M., van Boekel, R., Wang, W., Carmona, A., Sicilia-Aguilar, A., Henning, Th., 2009, *A&A*, 504, 461  
 Fressin, F. et al., 2013, *ApJ*, 766, 81  
 Furlan, E., et al., 2009, *ApJ*, 703, 1964  
 Gorti, U., Dullemond, C. P., Hollenbach, D., 2009, *ApJ*, 705, 1237  
 Greene, T. P., Lada, C. J., 1996, *AJ*, 112, 2184  
 Gullbring E., Hartmann L., Briceño C., Calvet N., 1998, *ApJ*, 492, 323  
 Harris, R. J., Andrews, S. M., Wilner, D. J., Kraus, A. L., 2012, *ApJ*, 751, 115  
 Hartigan, P., Kenyon, S. F., Hartmann, L., Strom, S. E.,



- Edwards, S., Welty, A. D., Stauffer, J., 1991, *ApJ*, 382, 617
- Hartigan P., Edwards S., Ghandour L., 1995, *ApJ*, 452, 736
- Hartmann L., 2001, *AJ*, 121, 1030
- Hartmann L., Calvet N., Gullbring E., D'Alessio P., 1998, *ApJ*, 495, 385
- Huelamo, N., Lacour, S., Tuthill, P., Ireland, M., Kraus, A., Chauvin, G., 2011, *A&A*, 528, L7
- Jensen E. L. N., Mathieu R. D., Fuller G. A., 1996, *ApJ*, 458, 312
- Jensen E. L. N., Mathieu R. D., Fuller G. A., 1994, *ApJ*, 429, L29
- Kelly, B., 2007, *ApJ*, 665, 1489
- Kenyon S. J., Hartmann L., 1995, *ApJS*, 101, 117
- Kim, K. H., et al., 2009, *ApJ*, 700, 1017
- Kim, K. H., et al., 2013, *ApJ*, 769, 149
- Kraus, A. L., Ireland, M. J., 2012, 745, 5
- Kraus, A., Ireland, M. J., Martinache, F., Hillenbrand, L. A., 2011, *ApJ*, 731, 8
- Lubow S. H., D'Angelo G., 2006, *ApJ*, 641, 526
- Lubow S. H., Seibert M., Artymowicz P., 1999, *ApJ*, 526, 1001
- Luhman, K. L., Rieke, G. H., 1999, *ApJ*, 525, 440
- Luhman, K. L., Briceño, C., Stauffer, J. R., Hartmann, L., Barrado y Navascués, D., Caldwell, N., 2003, *ApJ*, 590, 348
- Manara, C. F., Testi, L., Natta, A., Rosotti, G., Benisty, M., Ercolano, B., Ricci, L., 2014, *A&A*, 568, 18
- Manara, C. F., Robberto, M., Da Rio, N., Lodato, G., Hillenbrand, L. A., Stassun, K. G., Soderblom, D. R., 2012, *ApJ*, 755, 154
- Marsh K. A., Mahoney M. J., 1992, *ApJ*, 395, L115
- McClure, M. K. et al. 2010, *ApJS*, 188, 75
- Mendigutía, et al., 2012, *A&A*, 543, 59
- Motte, F., André, P., Neri, R., 1998, *A&A*, 336, 150
- Muzerolle, J., Calvet, N., Hartmann, L., 1998, *ApJ*, 492, 743
- Muzerolle J., Hillenbrand L., Calvet N., Briceño C., Hartmann L., 2003, *ApJ*, 592, 266
- Najita, J. R., Strom, S. E., Muzerolle, J., 2007, *MNRAS*, 378, 369
- Najita, J., R., Crockett, N., Carr, J. S., 2008, *ApJ*, 687, 1168
- Natta, A., Testi, L., Randich, S., 2006, *A&A*, 452, 245
- Nguyen, D. C., Scholz, A., van Kerkwijk, M. H., Jayawardhana, R., Brandeker, A., 2009, *ApJ*, 694, L153
- Nuernberger, D., Brandner, W., Yorke, H. W., Zinnecker, H., 1998, *A&A*, 330, 549
- Owen, J. E., 2014, 789, 59
- Owen, J. E., Ercolano, B., Clarke, C. J., Alexander, R. D., 2010, *MNRAS*, 401, 1415
- Pascucci, I., Sterzik, M., 2009, *ApJ*, 702, 724
- Patience, J., Akeson, R. L., Jensen, E. L. N. 2008, *ApJ*, 677, 616
- Petigura E. A., Howard A. W., Marcy G. W., 2013, *PNAS*, 110, p. 19273
- Quillen A. C., Blackman E. G., Frank A., Varnière P., 2004, *ApJ*, 612, L137
- Ratzka, T., Köhler, R., Leinert, Ch., 2005, *A&A*, 437, 611
- Reipurth, B., Zinnecker, H., 1993, *A&A*, 278, 81
- Ressler, M. E., Barsony, M., 2003, *ApJ*, 584, 832
- Rice W. K. M., Wood K., Armitage P. J., Whitney B. A., Bjorkman J. E., 2003, *MNRAS*, 342, 79
- Rice W. K. M., Armitage P. J., Wood K., Lodato G., 2006, *MNRAS*, 373, 1619
- Ricci, L., Testi, L., Natta, A., Brooks, K. J., 2010, *A&A*, 512, 15
- Rigliaco, E., Natta, A., Testi, L., Randich, S., Alcalà, J. M., Covino, E., Stelzer, B., 2012, *A&A*, 548, 56
- Rosotti, G. P., Ercolano, B., Owen, J. E., Armitage, P. J., 2013, *MNRAS*, 430, 1392
- Sacco, G. G., et al. 2012, *ApJ*, 747, 142
- Salyk, C., Herczeg, G. J., Brown, J. M., Blake, G. A., Pontoppidan, K. M., van Dishoeck, E. F., 2013, *ApJ*, 769, 21
- Shakura, N. I., Sunyaev, R. A., 1973, *A&A*, 24, 337
- Sicilia-Aguilar, A., Henning, Th., Hartmann, L. W., 2010, *ApJ*, 710, 597
- Skrutskie M. F., Dutkevitch D., Strom S. E., Edwards S., Strom K. M., Shure M. A., 1990, *AJ*, 99, 1187
- Siess, L., Dufour, E., Forestini, M., 2000, *A&A*, 358, 593
- Stanke, T., Smith, M. D., Gredel, R., Khanzadyan, T., 2006, *A&A*, 447, 609
- Strom K. M., Strom S. E., Edwards S., Cabrit S., Skrutskie M. F., 1989, *AJ*, 97, 1451
- Tanaka, H., Himeno, Y., Ida, S., 2005, *ApJ*, 625, 414
- Valenti, J. A., Basri, G., Johns, C. M., 1993, *AJ*, 106, 2024
- White R. J., Ghez A. M., 2001, *ApJ*, 556, 265
- Williams, J. P., Cieza, L. A., 2011, *ARAA*, 49, 67
- Zhu, Z., Nelson, R. P., Hartmann, L., Espaillat, C., Calvet, N., 2011, *ApJ*, 729, 47
- Zhu, Z., Nelson, R., P., Dong, R., Espaillat, C., Hartmann, L., 2012, *ApJ*, 755, 6

This paper has been typeset from a  $\text{\TeX}$ / $\text{\LaTeX}$  file prepared by the author.

**Table 1.** Ophiuchus Stellar Accretion Rates and Disk Masses

| Source<br>(1) | SpT<br>(2) | Mult<br>(3) | $L_*$<br>(4) | $\log R_*$<br>(5) | $\log M_*$<br>(6) | $\log \dot{M}_*$<br>(7) | $\log M_d$<br>(8) | $\log M_{d,\text{fit}}$<br>(9) | Ref<br>(10) | $A_V$<br>(11) | Type<br>(12) | Other Name<br>(13)   |
|---------------|------------|-------------|--------------|-------------------|-------------------|-------------------------|-------------------|--------------------------------|-------------|---------------|--------------|----------------------|
| IRS2          | K3.5       | B           | 1.66         | 0.29              | 0.16              | < -7.29                 | < -3.58           |                                |             | 16.9          | N            | YLW19                |
| SR4           | K4.5       | S           | 1.31         | 0.28              | 0.08              | -7.28                   | -2.37             |                                |             | 2.2           | N            | AS206/IRS12          |
| GSS26         | K7         | S           | 8.14         | 0.76              | -0.09             | < -7.73                 | -2.13             |                                |             | 21.9          | N            | -                    |
| EL18          | M1         | B           | 2.14         | 0.55              | -0.33             | < -8.01                 | < -3.14           |                                |             | 9.9           | N            | GSS29                |
| DoAr24        | K5         | S           | 1.23         | 0.29              | 0.02              | -8.88                   | < -2.59           |                                |             | 3.5           | N            | GSS28/HBC638         |
| EL20          | M0         | S           | 1.97         | 0.50              | -0.27             | -6.82                   | -2.15             | -1.54                          | A09         | 14.2          | N            | VSSG1                |
| GY11          | M6         | S           | 0.002        | -0.78             | -1.13             | < -12.68                | < -2.48           |                                |             | 4.2           | N            | -                    |
| DoAr25        | K5         | S           | 1.52         | 0.33              | 0.04              | < -9.55                 | -1.71             | -0.87                          | A09         | 3.4           | O            | WSB29/GY17           |
| LFAM3         | M0         | S           | 0.31         | 0.09              | -0.24             | -8.90                   | -1.83             |                                |             | 16.1          | O            | GY21                 |
| EL24          | K5         | S           | 5.10         | 0.60              | 0.04              | -6.43                   | -1.65             | -0.93                          | A09         | 8.7           | N            | WSB31                |
| VSSG27        | K6         | S           | 1.83         | 0.40              | -0.04             | -7.02                   | < -2.82           |                                |             | 24.0          | N            | GY51                 |
| WSB37         | M5         | B           | 0.21         | 0.19              | -0.69             | < -9.58                 | < -2.42           |                                |             | 2.5           | N            | GY93                 |
| IRS17         | K3         | S           | 1.14         | 0.20              | 0.17              | < -9.33                 | < -2.58           |                                |             | 20.3          | N            | WL7/GY98/WLY2-17     |
| EL26          | M0         | S           | 1.71         | 0.47              | -0.28             | -8.04                   | -2.93             |                                |             | 7.5           | N            | GSS37AB/GY110        |
| EL27          | M0         | S           | 1.28         | 0.40              | -0.28             | -7.10                   | -1.57             | -0.84                          | A09         | 14.8          | N            | GSS39/GY116          |
| WSB38         | G3.5       | B           | 5.46         | 0.36              | 0.07              | -8.64                   | < -2.95           |                                |             | 7.0           | N            | VSS27AB/ROXs16       |
| WL18          | K6.5       | S           | 0.27         | 0.00              | -0.10             | -7.84                   | -2.45             |                                |             | 10.5          | N            | GY129                |
| WL14          | M4         | S           | 0.14         | 0.06              | -0.62             | < -10.20                | -2.28             |                                |             | 15.8          | O            | GY172                |
| WL16          | A1         | S           | 250.         | 0.79              | 0.65              | -5.26                   | < -3.93           |                                |             | 31.0          | N            | GY182/YLW5           |
| IRS29         | M4         | B           | 0.63         | 0.39              | -0.58             | < -9.90                 | -3.18             |                                |             | 17.8          | N            | WL1AB/GY192          |
| WL10          | K7         | S           | 0.96         | 0.29              | -0.12             | -8.63                   | < -3.03           |                                |             | 11.5          | N            | GY211                |
| SR21          | F4         | S           | 16.54        | 0.49              | 0.16              | < -8.51                 | -2.40             | -2.22                          | A11         | 6.9           | HT           | EL30/VSSG23          |
| WL11          | M0         | S           | 0.10         | -0.15             | -0.27             | -10.33                  | < -2.71           |                                |             | 11.5          | N            | GY229                |
| IRS34         | M0         | B           | 1.07         | 0.36              | -0.27             | < -8.41                 | < -2.74           |                                |             | 24.7          | N            | GY239                |
| IRS39         | M1.5       | S           | 1.05         | 0.41              | -0.38             | < -8.97                 | -2.62             |                                |             | 18.4          | N            | WL4/GY247            |
| IRS42         | K7         | S           | 7.29         | 0.73              | -0.10             | < -7.57                 | < -2.51           |                                |             | 25.0          | N            | GY252                |
| YLW16C        | M1         | S           | 1.39         | 0.45              | -0.34             | -7.49                   | -2.30             |                                |             | 22.5          | N            | GY262                |
| EL31          | M4         | B           | 0.87         | 0.46              | -0.58             | < -8.59                 | < -3.02           |                                |             | 11.7          | N            | WL13/VSSG25/GY267    |
| EL32          | K6.5       | S           | 1.75         | 0.41              | -0.07             | < -8.65                 | < -2.41           |                                |             | 21.1          | N            | IRS45/GY273          |
| EL33          | M3         | B           | 4.88         | 0.80              | -0.47             | < -7.70                 | < -2.94           |                                |             | 24.1          | N            | IRS47/GY279          |
| GY284         | M3.2       | S           | 0.12         | 0.00              | -0.56             | < -10.31                | -1.62             |                                |             | 6.0           | O            | -                    |
| ROXs25        | K7         | S           | 3.07         | 0.55              | -0.11             | -7.20                   | -2.71             |                                |             | 11.6          | N            | GY292                |
| IRS49         | K5.5       | S           | 2.16         | 0.43              | 0.22              | -8.30                   | -2.70             |                                |             | 10.5          | N            | GY308                |
| WSB52         | K5         | S           | 0.60         | 0.27              | -0.34             | -8.26                   | -2.15             | -2.15                          | A10         | 5.0           | N            | GY314                |
| SR9           | K5         | B           | 2.10         | 0.40              | 0.04              | -8.43                   | < -3.12           |                                |             | 1.6           | N            | AS207/GY319/IRS52    |
| SR10          | M2         | S           | 0.33         | 0.18              | -0.43             | -8.30                   | < -2.49           |                                |             | 1.3           | N            | GY400/HBC265         |
| WSB60         | M4.5       | S           | 0.20         | 0.16              | -0.65             | -8.59                   | -1.74             | -1.55                          | A11         | 3.9           | H            | YLW58/B162816-243657 |
| SR20          | G7         | B           | 8.71         | 0.49              | 0.07              | < -8.41                 | < -3.30           |                                |             | 6.0           | N            | HBC643               |
| SR13          | M4         | B           | 0.40         | 0.29              | -0.59             | -8.46                   | -2.09             | -1.92                          | A10         | 0.0           | N            | HBC266               |
| AS205A        | K5         | S           | 4.00         | 0.54              | 0.04              | -6.47                   | -1.71             | -1.54                          | A10         | 2.9           | N            | -                    |
| AS209         | K5         | S           | 1.50         | 0.33              | 0.04              | -7.29                   | -1.76             | -1.60                          | A10         | 0.9           | N            | -                    |
| DoAr44        | K3         | S           | 1.90         | 0.31              | 0.20              | -8.04                   | -2.11             | -2.15                          | A11         | 3.3           | HT           | ROXs44               |
| SR24S         | K2         | S           | 4.40         | 0.46              | 0.30              | -7.15                   | -1.88             | -1.35                          | A11         | 7.0           | H            | -                    |
| WaOph6        | K6         | S           | 2.90         | 0.50              | -0.04             | -6.64                   | -2.02             | -1.11                          | A10         | 3.6           | N            | -                    |

Column 2: Spectral types from McClure et al. (2010), Andrews & Williams (2007a, 2007b), Andrews et al. (2009, 2010). Column 3:

Sources with a companion within  $1''$  are classified as binaries (Reipurth & Zinnecker 1993, Barsony et al. 2005; Ratzka et al. 2005). Columns 4 and 12: Stellar luminosity (in  $L_\odot$ ) and  $A_V$  from McClure et al. (2010) and M. McClure (2014, private communication) except for WL16 (Ressler & Barsony 2003), WL14 (Luhman & Rieke 1999), GY11 (Cushing et al. 2000), EL24, WSB52, SR13, AS205A, AS209, SR24S, WaOph6 (Andrews et al. 2010). Columns 5 and 6: Derived stellar radius (in  $R_\odot$ ) and stellar mass (in  $M_\odot$ ). Column 7: Stellar accretion rate derived from Natta et al. (2006) measurements using the stellar parameters from McClure et al. (2010) (see text for details). Column 8: Disk mass (in  $M_\odot$ ) estimated from optically thin, isothermal approximation (see §2 for details). Column 9: Alternate disc mass estimate from a fit to the SED and resolved millimeter visibilities. Column 10: Reference for  $M_{d,\text{fit}}$ : A09 = Andrews et al. (2009); A10 = Andrews et al. (2010); A11 = Andrews et al. (2011). Column 12: Source type, where N= normal T Tauri star; T= transition disc SED; H= submillimeter cavity; O= outlier.

**Table 2.** Taurus Stellar Accretion Rates and Disk Masses

| Source<br>(1) | SpT<br>(2) | $\log M_*$<br>(3) | $\log \dot{M}_*$<br>(4) | $\log M_d$<br>(5) | $\log M_{d,\text{fit}}$<br>(6) | Ref $M_{d,\text{fit}}$<br>(7) | Type<br>(8) |
|---------------|------------|-------------------|-------------------------|-------------------|--------------------------------|-------------------------------|-------------|
| AATau         | K7         | -0.10             | -8.48                   | -2.04             | -1.52                          | A07                           | N           |
| BPTau         | K7         | -0.10             | -7.54                   | -2.25             |                                |                               | N           |
| CITau         | K7         | -0.10             | -7.19                   | -1.84             | -1.40                          | A07                           | N           |
| CWTau         | K3         | 0.20              | -7.61                   | -2.27             |                                |                               | N           |
| CXTau         | M2.5       | -0.44             | -8.97                   | -2.77             |                                |                               | N           |
| CYTau         | M1.5       | -0.36             | -8.12                   | -1.85             |                                |                               | N           |
| DETau         | M1         | -0.41             | -7.59                   | -2.39             |                                |                               | N           |
| DGTau         | K7         | -0.04             | -6.30                   | -1.43             |                                |                               | N           |
| DHTauA        | M1         | -0.32             | -8.30                   | -2.54             | -2.52                          | A07                           | N           |
| DKTau         | M0         | -0.15             | -7.42                   | -2.69             |                                |                               | N           |
| DLTau         | K7         | -0.09             | -6.79                   | -1.61             | -1.00                          | A07                           | N           |
| DMTau         | M1         | -0.33             | -7.95                   | -1.72             | -1.40                          | A11                           | T           |
| DNTau         | M0         | -0.22             | -8.46                   | -1.93             | -1.22                          | A07                           | N           |
| DOTau         | M0         | -0.33             | -6.85                   | -1.88             |                                |                               | N           |
| DRTau         | K7         | 0.08              | -6.50                   | -1.89             | -2.00                          | A07                           | N           |
| DSTau         | K5         | 0.02              | -7.89                   | -2.62             |                                |                               | N           |
| FMTau         | M0         | -0.22             | -8.45                   | -2.63             |                                |                               | N           |
| FYTau         | K7         | 0.07              | -7.41                   | -2.80             |                                |                               | N           |
| FZTau         | M0         | -0.35             | -7.32                   | -2.77             |                                |                               | N           |
| GITau         | K7         | -0.10             | -7.69                   | -2.81             |                                |                               | N           |
| GKTau         | K7         | -0.11             | -8.19                   | -3.44             |                                |                               | N           |
| GMAur         | K3         | 0.13              | -8.02                   | -1.66             | -1.15                          | A11                           | T           |
| GOTau         | M0         | -0.20             | -7.93                   | -1.98             | -0.74                          | A07                           | N           |
| HKTau         | M0.5       | -0.27             | -7.27                   | -2.27             |                                |                               | N           |
| HNTau         | K5         | -0.04             | -8.41                   | -2.64             |                                |                               | N           |
| HOTau         | M0.5       | -0.25             | -8.86                   | -2.34             |                                |                               | N           |
| IPTau         | M0         | -0.22             | -9.10                   | -2.83             |                                |                               | N           |
| IQTau         | M0.5       | -0.27             | -7.55                   | -2.06             |                                |                               | N           |
| LkCa15        | K5         | 0.02              | -8.87                   | -1.74             | -1.26                          | A11                           | T           |
| RWAurA        | K3         | 0.18              | -7.12                   | -2.52             |                                |                               | N           |
| RYTau         | K1         | 0.44              | -7.11                   | -1.92             | -1.70                          | A07                           | N           |
| UXTauA        | K2         | 0.20              | -9.00                   | -2.22             | -2.15                          | A11                           | T           |
| V836Tau       | K7         | -0.08             | -8.98                   | -2.33             |                                |                               | N           |

Column 3: Stellar mass (in  $M_\odot$ ). Column 4: Stellar accretion rate (in  $M_\odot \text{ yr}^{-1}$ ).

Column 5, 6: Disk mass (in  $M_\odot$ ). Column 7: A07 = Andrews & Williams (2007b); A11 = Andrews et al. (2011). Column 8: Source type, where N= normal T Tauri star; T= transition disc.